Novel gold catalysts for the direct conversion of ethanol into C_{3+} hydrocarbons

S.A. Nikolaev [a,*], A.V. Chistyakov [b], M.V. Chudakova [b], E.P. Yakimchuk [c], V.V. Kriventsov [c], M.V. Tsodikov [b]

[a] Faculty of Chemistry, Moscow State University, Leninskie Gory 1, Moscow 119991, Russia
[b] Topchiev Institute of Petrochemical Synthesis RAS, Leninskii pr. 29, Moscow 119991, Russia
[c] Boreskov Institute of Catalysis RAS, Pr. Akademika Lavrentieva 5, Novosibirsk 630090, Russia

ABSTRACT

The catalytic properties of the M/Al_2O_3 (M = NiO, Au, NiO/Au) catalysts were investigated during the conversion of ethanol into C_{3+} hydrocarbons at 623 K. The NiO clusters with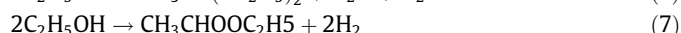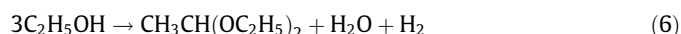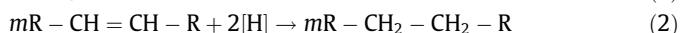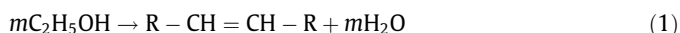 a size of 3.5 nm possess low selectivity (12.73%) and low turnover frequency (TOF) $0.051\ s^{-1}$. By decreasing the size of the Au particles from 15.1 to 5 nm, the TOF increased from 0.095 to $0.384\ s^{-1}$. The reaction with the 5-nm Au particles afforded C_{3+} hydrocarbons with a selectivity of 11.69%. Growing the Au particles by aggregating and/or forming the mixed NiO/Au particles resulted in an increased C_{3+} hydrocarbons selectivity, up to 34.19%. The peculiarities of the reaction mechanism are discussed, with the specific surface and electronic features of the prepared catalysts being considered.

© 2012 Elsevier Inc. All rights reserved.

1. Introduction

Bioethanol is an alcohol produced by fermentation of sugar cane, starch, and algae [1–3]. It can be used as a fuel for vehicles [1–6]. However, there are some obstacles to the wide application of alcohol-based biofuel. Using the pure bioethanol is not possible without changing the overall engine design and, accordingly, without changing the entire production line. The fuel efficiencies for hybrid cars using the E85 mixture (85% bioethanol, 15% gasoline) are only 75% those of standard cars. Converting of bioethanol into the common gasoline components (C_{3+} hydrocarbons) is the most promising way of its application in the transport industry [4]. The reductive dehydration (Eqs. (1) and (2)) over Pd- or Pt-catalysts allows ethanol to be transformed into C_{3+} alkane fraction [4–6]. The important feature of the reductive dehydration is the direct formation of hydrogen, which is required for reducing the hydrocarbon backbone. Hydrogen is generated directly from ethanol via reactions presented in Eqs. (3)–(8).

$$mC_2H_5OH \rightarrow R-CH=CH-R + mH_2O \tag{1}$$
$$mR-CH=CH-R + 2[H] \rightarrow mR-CH_2-CH_2-R \tag{2}$$
$$C_2H_5OH \rightarrow CH_4 + CO + H_2 \tag{3}$$
$$C_2H_5OH + H_2O \rightarrow 2CO + 4H_2 \tag{4}$$
$$C_2H_5OH \rightarrow CH_3CHO + H_2 \tag{5}$$

$$3C_2H_5OH \rightarrow CH_3CH(OC_2H_5)_2 + H_2O + H_2 \tag{6}$$
$$2C_2H_5OH \rightarrow CH_3CHOOC_2H5 + 2H_2 \tag{7}$$
$$CO + H_2O \rightarrow CO_2 + H_2 \tag{8}$$
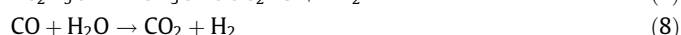
When compared to Pd and Pt catalytic systems, gold nanoparticles are more effective for catalyzing oxidation, isomerization, and hydrogenation reactions under mild conditions [7–13]. Notably, nickel–gold catalysts are thought to possess synergistic activity and stability when converting a variety of hydrocarbons such as n-butane [9], ethynylbenzene [10], ethyne [11], and 2,4-dichlorophenol [12]. These promising reports indicate gold nanoparticles and nickel–gold clusters as potential catalysts for the reductive ethanol dehydration (Eqs. (1) and (2)).

2. Experimental

2.1. Catalyst preparation

Gamma Al_2O_3 with $S = 160\ m^2/g$ was used as a support for metal nanoparticles. Au/Al_2O_3 catalysts were produced by deposition–precipitation as described in [10,11]. In typical experiment, an aqueous solution of $HAuCl_4$ was adjusted to pH = 7.0 by adding NaOH (0.1 M), and then, the support was dispersed in the solution with stirring for 1 h. This precursor was washed to remove Cl^-, dried in air at 298 K for 24 h and calcined in air at 623 K for 3 h. NiO/Al_2O_3 catalyst was produced by impregnating Al_2O_3 (calcined at 623 K for 3 h) with an aqueous solution of $Ni(NO_3)_2$, followed by calcination at 623 K for 3 h. NiO/Au catalysts were produced by

impregnating Au/Al$_2$O$_3$ catalysts with an aqueous solution of Ni(NO$_3$)$_2$, followed by calcination at 623 K for 3 h. The catalysts were reduced in a stream of H$_2$ at 723 K for 12 h before use.

2.2. Catalyst characterization

The metal content of the catalysts was determined by atomic absorption on a Thermo iCE 3000 AA spectrometer. The relative error of this method was within ±1%. Transmission electron microscopy (TEM) and energy-dispersive X-ray (EDX) analysis of catalysts were carried out on a JEOL JEM 2100F/UHR microscope with 0.1-nm resolution and a JED-2300 X-ray spectrometer, respectively. The size of spherical (SPH) and distorted (DIS) particles was calculated as diameter and maximum linear size, respectively. For each catalyst, 300–380 particles were processed to determine the particle size distribution. The mean particle size was determined as the average size of the most frequent particles. The concentration of SPH particles in the catalyst was calculated as C(SPH) = n(SPH) × N × 100%, where n(SPH) is the number of SPH particles, and N(300–380) is the number of processed particles. The concentration of DIS particles was calculated in the same manner. X-ray diffraction (XRD) analysis was carried out on a Rigaku D/MAX 2500 instrument using CuKα radiation with a step size of 0.02° two-theta (2θ) ranging from 35° to 70°. The EXAFS and XANES spectra (Ni—K, Au—L$_3$) for all the catalysts studied were obtained at the EXAFS Station of the Siberian Synchrotron Radiation Center (SSRC, Novosibirsk). The VEPP-3 storage ring (E = 2 GeV, $I \sim$ 90 mA) was used as the radiation source. The X-ray energy was monitored with a channel-cut Si (1 1 1) monochromator. The EXAFS and XANES spectra were recorded using the ionization chambers and a fluorescence detector with step of ∼1.5 eV and ∼0.3 eV, respectively. The EXAFS spectra were treated using standard procedures [14]. The atomic radial distribution functions (RDFs) were calculated from the EXAFS spectra in $k^3\chi(k)$ as the modulus of their Fourier transform using a wave number interval of 3.0–12.0 Å^{-1}. A curve-fitting procedure with VIPER and EXCURV92 codes [14,15] was employed to determine the distances (R) and coordination numbers (CNs) in similar wave number intervals after preliminary Fourier filtering using the known XRD literature data for the bulk compounds. The Debye–Waller factors were fixed as $2\sigma^2$ = 0.009–0.012 Å^2.

2.3. Reductive dehydration of ethanol

Analytical grade ethanol (99%) was used without further purification. The reductive dehydration of ethanol was performed in a flow-circulation unit with a vertical fixed-bed reactor. The standard reaction conditions were the following: temperature (623 K), pressure (50 bar of Ar), catalyst (12 g), time (3 h), ethanol feed (0.6 h^{-1}), and gas circulation rate (50 cm^3/min). The liquid products were collected in a water-cooled separator, and gaseous products with gas carrier (Ar) were brought back to the reactor with circulation piston pump. Qualitative and quantitative analyses of the C$_1$—C$_5$ hydrocarbon gases were performed by gas–liquid chromatography (GLC) with a Kristall-4000 M chromatograph (detector: FID, carrier gas: He, column: HP-PLOT/Al$_2$O$_3$, 50 m × 0.32 mm). GLC analyses of CO, CO$_2$, and H$_2$ were performed with a Kristall-4000 chromatograph (detector: TCD, carrier gas: Ar, column: SKT, 1.5 m × 4 mm). The qualitative composition of the C$_{6+}$ hydrocarbons in the aqueous and organic phases was identified by gas chromatography–mass spectrometry (GC–MS) using a MSD 6973 – and an Automass-150 spectrometer – (EI = 70 eV, catalyst volume = 1 μl, columns: HP-5MS, 50 m × 0.32 mm and CPSil-5, 25 m × 0.15 mm). The quantitative content of the organic compounds was determined by GLC using a Varian 3600 chromatograph (detector: FID, carrier gas: He, column: Chromtec SE-30,

25 m × 0.25 mm). The ethanol content in the aqueous phase was determined by GC–MS using the absolute calibration method on the ratio of alcohol to water integral signals. Ethanol conversion (α) was determined as $\sum v_i(C_xH_yO_z) \times v_0(C_2H_5OH)^{-1} \times 100\%$, where $\sum v_i(C_xH_yO_z)$ is the sum of the molar amounts of all products and $v_0(C_2H_5OH)$ is the initial molar amount of alcohol in the reaction mixture. Turnover frequency (TOF) was calculated as $\sum v_i(C_xH_yO_z) - \times v(M)^{-1} \times \tau^{-1}$, where τ is the reaction time and $v(M)$ is the molar amount of the metal deposited by the catalyst. Selectivity (S) was calculated as $\sum m_i(C_3–C_8) \times \sum m_i(C_xH_yO_z)^{-1} \times 100\%$, where $\sum m_i(C_3–C_8)$ is the sum of the hydrocarbon masses in the targeted fraction (C$_3$–C$_8$).

3. Results and discussion

Some gold, nickel, and nickel–gold catalysts (Table 1, No. 1–9) were prepared and studied herein. The monometallic nickel catalyst (No. 1) was gray in color. The monometallic gold catalysts (No. 2–4) were lilac in color, in good agreement with the color reported for other gold catalysts obtained by deposition–precipitation [16,17]. The bimetallic catalysts (No. 5–9) were purple in color. The structure of the catalysts No. 1–9 is presented in Table 1 and Figs. 1–12.

3.1. Oxidation states and local structures of the supported metal clusters

The XANES (Au—L$_3$) spectra for the Au/Al$_2$O$_3$ (No. 3) and NiO/Au/Al$_2$O$_3$ (No. 7) are presented in Fig. 1a–d. The spectra of the unreduced catalysts (Fig. 1a and c) were similar to the spectrum of a gold foil (Fig. 1e). A low intensity white line corresponding to cationic gold Au$^{\delta+}$ was observed in the unreduced catalyst spectra (Fig. 1a, c and f). The presence of Au$^{\delta+}$ could be due to residue from the gold precursor HAuCl$_4$, interaction of gold nanoparticles with oxygen on the support surface [8,17] or, in the case of Au—Ni catalyst, transfer of electron density from gold to nickel [10,11]. The amount of Au$^{\delta+}$ in the unreduced Au/Al$_2$O$_3$ (No. 3) was ∼17% of the total gold content. The amount of Au$^{\delta+}$ in the unreduced NiO/Au/Al$_2$O$_3$ (No. 7) was ∼10% of the total gold content. The white line in the Au and NiO/Au catalysts disappeared after sequential reducing with hydrogen and the reductive dehydration reaction (Fig. 1b and d), causing the XANES (Au—L$_3$) spectra to become identical to that of the Au^0 foil spectrum (Fig. 1e).

The gold RDF curves for the Au/Al$_2$O$_3$ (No. 3) and NiO/Au/Al$_2$O$_3$ (No. 7) are presented in Fig. 2a–d. Low amplitude peaks were observed on the RDF curves in the 1.4–2.1 Å region for the unreduced catalysts (Fig. 2a and c). These peaks corresponded to Au—O oxide bonds (∼2 Å) [18]. Intensive peaks were also present in the 2.1–3.5 Å region for the unreduced catalysts (Fig. 2a and c). These peaks corresponded to the Au—Au bond distance in the zero-valent metal (∼2.86 Å) [19]. The Au—Au peak amplitudes of the catalysts (Fig. 2a and c) were smaller than those in the bulk gold due to dispersion

Table 1
Structure of catalysts No. 1–9 before (a) and after reaction (b): metal content (M); content of spherical (SPH) and distorted (DIS) particles, mean cluster size (D).

No.	[Au] (wt.%)	[Ni] (wt.%)	[SPH]^a (%)	D_{SPH}^a (nm)	[SPH]^b (%)	D_{SPH}^b (nm)	[DIS]^b (%)	D_{DIS}^b (nm)
1	0	0.15	100	3	99.5	3.5	0.5	8
2	0.1	0	99	3.2	97	5	3	11
3	0.21	0	100	5.1	82	8	18	14.4
4	0.5	0	100	7.2	68	13	32	15.1
5	0.21	0.02	100	6.2	73	6.4	27	13.2
6	0.21	0.07	100	6.3	66	6.7	34	16.2
7	0.21	0.21	100	6.5	47	7.1	53	16.4
8	0.5	0.15	100	7.9	55	11.1	45	17
9	0.1	0.03	100	3.4	56	4.5	44	14.8